NASA-TP-1800 19810022739

Development and Design of Three Monitoring Instruments for Spacecraft Charging

John C. Sturman

NASA

NASA Technical Paper 1800

Development and Design of
Three Monitoring Instruments
for Spacecraft Charging

John C. Sturman
Lewis Research Center
Cleveland, Ohio

Summary

A set of three instruments has been developed that can provide early detection of potentially dangerous geomagnetic substorm conditions and monitor the spacecraft response. The set consists of a sensor that measures the characteristic energy of collected electrons or ions from $+100$ to $-20,000$ volts, a logarithmic current density sensor that measures local electron flux by measuring currents from 10^{-9} to 10^{-5} amperes, and a transient events counter that counts the spurious pulses from electrostatic discharges that couple into the spacecraft wiring harness. The counted pulses are those that are large enough to cause circuit malfunction. Design details and performance characteristics of the three instruments are given. Size, weight, and power requirements have been minimized. Total weight and power for all three instruments is 1.36 kilograms and 0.75 watt. The instruments are also suitable for laboratory use.

Introduction

Anomolous behaviour of the electrical systems of geosynchronous spacecraft has been attributed to spacecraft charging (refs. 1 to 4). These anomalies have ranged from uncommanded electronic switching in components to total system failures. This results from the collection of energetic electrons from a geomagnetic substorm environment on satellite surfaces. Thermal control surfaces and solar arrays are most subject to charge buildup since they are excellent insulators and can comprise a large portion of the total satellite surface area. The environmental electron flux will charge these insulating surfaces sufficiently negatively to reduce the net charging current to zero. In sunlight these surfaces lose electrons by photoemission, partially balancing collected electrons and limiting voltage buildup to a few hundred volts. During eclipse, or on shadowed surfaces, there is no adequate discharge mechanism available, and charging to several kilovolts negative is possible (refs. 5 to 9). This was substantiated by experimental evidence on the ATS-5 and ATS-6 satellites (refs. 10 and 11). Many of the observed anomalies have occurred during the midnight-to-dawn portion of satellite orbit when discharge is difficult or impossible (ref. 12).

When the charging voltage reaches the breakdown potential of the insulating material, an arc discharge will occur. It can involve considerable surface area and produce large current flows (refs. 12 to 14). These arcs produce electromagnetic interference, degrade thermal control surfaces by tracking and burning, and cause surface contamination (ref. 15). Most serious to the immediate function of the spacecraft are the large voltage transients induced in the wiring harness. These are conducted into onboard electronics systems. Depending on the transient voltage level, the effects can range from uncommanded switching of logic circuits to permanent damage or destruction of semiconductor devices.

During the past several years a number of research programs have addressed the problems of spacecraft charging using both ground simulation and satellite measurements (refs. 16 to 23). One of these is a comprehensive Air Force and NASA program that included ground simulation of charging conditions, materials testings, mathematical modeling, and the SCATHA (Spacecraft Charging at High Altitudes) satellite launched January 25, 1979 (refs. 24 to 26). The instruments to be described herein were developed as part of this program.

The minimum amount of information required to characterize the substorm environment and determine the satellite response to this environment is

(1) The flux density of charged particles incident on the spacecraft
(2) The energy of these charged particles
(3) The number and magnitude of transients induced in the satellite electrical harness.

The flux density is measured by a logarithmic nanoammeter connected to a bare metal collector plate. For the energy measurement it would be desirable to measure the energy spectral density of the incident electrons. However, such an instrument would be large, complex, and expensive. A simpler alternative is to measure the characteristic energy of the space plasma. The second instrument, a surface voltage sensor (SVS) approximates this. It measures the maximum voltage that a well-insulated, gold-plated electrode, mounted near the spacecraft surface reaches. The third instrument, the transient events counter or TEC, counts the number of discharge-induced pulses in the spacecraft wiring harness. The prototype instrument has four channels, each of which may be preset to a given threshold. Each
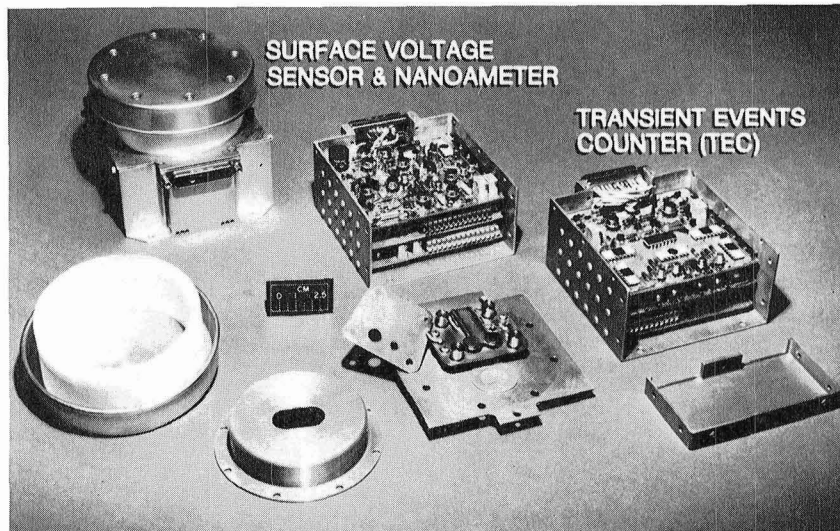
Figure 1. - Charging effects monitors.

channel can be used with a separate sense line to monitor transients in different sections of the harness, or it can be set to different thresholds to characterize the amplitude distribution of induced pulses in the same section. Correlating transients in several sections of the spacecraft wiring can also give some indication of the source of the discharge. This instrument is an improved version of the ones flown on the joint Canadian-American Communications Technology Satellite (CTS), launched January 17, 1976, and now called Hermes (ref. 27), and on the European Orbital Test Satellite (OTS), launched May 11, 1978.

These three instruments (shown in fig. 1) have been packaged into two units of minimal size and weight that can be added to any spacecraft to monitor charging conditions. Their value to the host satellite is the early warning of potentially dangerous charging conditions that they can give. In the event of a severe solar storm, the monitors can give minutes of warning to allow the spacecraft to reconfigure itself to protect it from damage. In addition, the data produced during periods of normal operation would aid in defining the space environment and its effects on satellites that would be valuable information for future designs.

Logarithmic Nonammeter

Requirements

The basic requirements for the nanoammeter were (1) that it be able to measure currents from -1×10^{-9} to -1×10^{-5} ampere with an accuracy of 5 percent of reading (This is equivalent to an electron flux of -2×10^{-11} to -2×10^{-7} A/cm^2 for a collector plate area of 50 cm^2, which is a practical size); (2) that its input impedance be low enough so that, at maximum input current, the collector plate would not be more than 1 volt off ground; and (3) that the output to telemetry be a single analog signal of 0 to 5 volts proportional to the log of negative input current. Table I gives the specifications that were achieved.

Design

The circuit design of the nanoammeter is shown in a functional diagram (fig. 2) and an electrical schematic (fig. 3). The input is protected by a gas surge suppressor (SVP-1) and a pair of FET diodes (CR-3). This protection is important since the current

TABLE I.—LOG NANOAMMETER SPECIFICATIONS

Current range, A	[a]-10^{-9} to -10^{-5}
Input impedance, kΩ	≤ 100
Plasma current range with 50 cm^2 collector, A/cm^2	$< -2 \times 10^{-11}$ to -2×10^{-7}
Accuracy (temperature compensated), percent	± 5
Operating temperature, °C	-40 to $+70$
Power supply, V dc:	
Input	28
Output	± 12
Circuit power at ± 12 V dc, mW	102
Size of single printed circuit card, cm	8.7 by 9.4
Output[b]: V dc, mW	0 to 5

[a]To -1×10^{-10} A with reduced accuracy.

[b]Analog signal proportional to log of input current.

collector plate would probably be on a spacecraft surface most subject to charging and could be subjected to large transient voltages in case of a discharge.

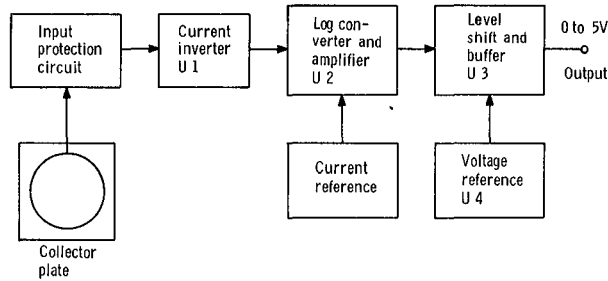The first active stage is a current inverter. It is required for the measurement of collected electron current because the following logarithmic stage, U2, will only accept positive input current. The inverting stage has a unity current gain over more than the full five-decade range of the instrument. Operation of this stage depends on the current-voltage characteristic of the matched transistor pair, Q1A and Q1B, which are connected as diodes. The negative input current flows through Q1A producing a voltage drop. If both halves of Q1 are perfectly matched, driving the voltage across Q1B to the same value as that across Q1A produces equal current flow in both Q1A and Q1B. Amplifier U1 does this, so that the negative input current is inverted, producing a positive output current of equal value. It is the logarithmic current-voltage relationship of Q1 that makes possible operation over more than five decades of current. The op-amp, U1, used in this stage has very low input current and offset voltage, which eliminates the need for trimming.

The second stage is the heart of the instrument. Most logarithmic circuits depend on the logarithmic
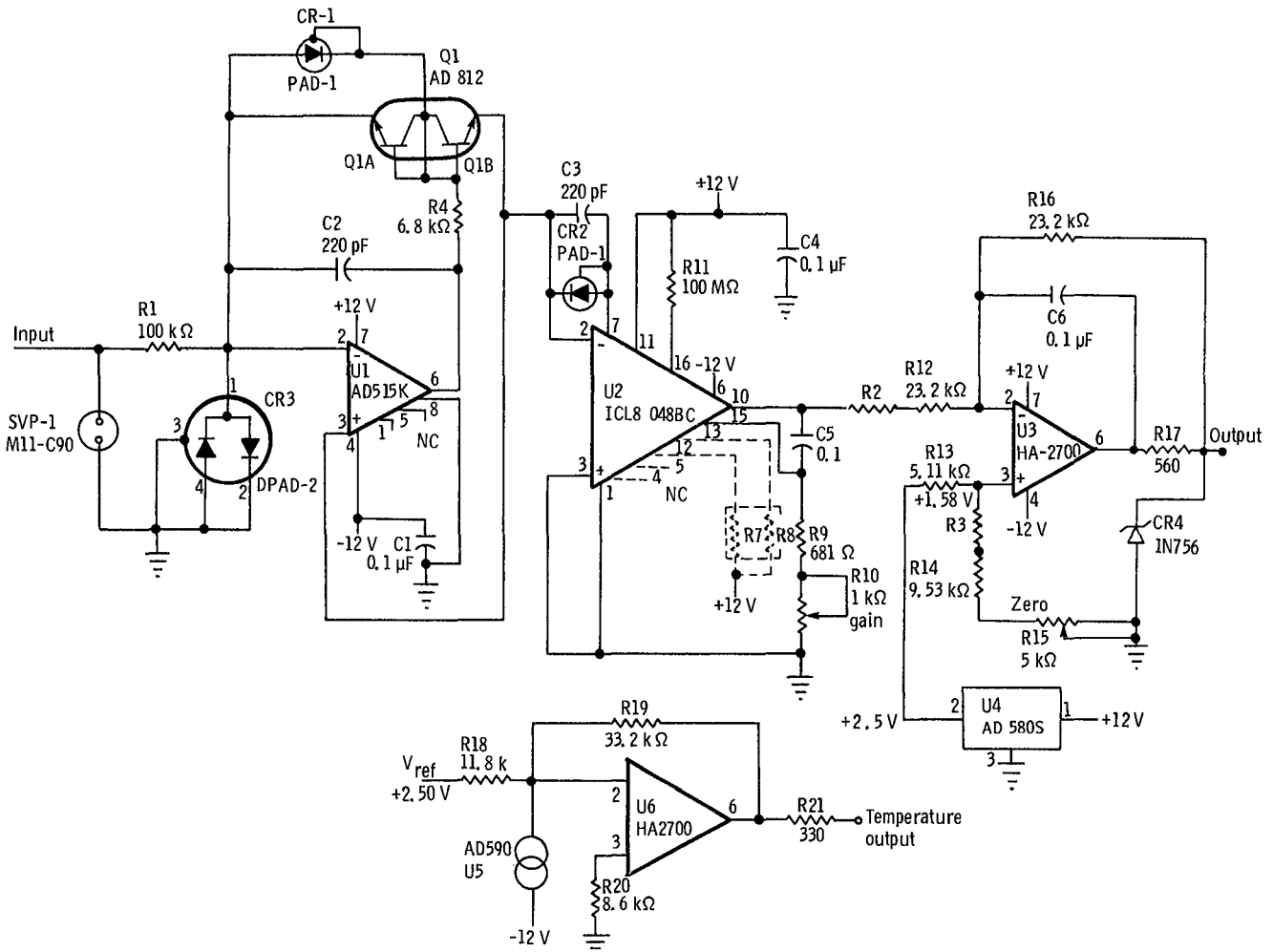

Figure 2. – Logarithmic nanoammeter functional diagram.

Figure 3. – Logarithmic nanoammeter schematic.

current-voltage characteristic of a silicon junction, which is temperature dependent. Circuit performance is then determined by how well this temperature dependence can be compensated for. Use of a monolithic logarithmic amplifier for U2 minimizes these temperature problems since both the logarithmic and compensation circuits are on the same chip and, therefore at the same temperature. This stage compares the input current with a reference current (pin 16) and produces an output proportional to the log of their ratio. The output is 1 volt per decade of input current and swings both positive and negative with respect to ground. Offset voltage trim is required and can be implemented using one fixed resistor (R7 or R8) as required.

Amplifier U3 is a unity gain buffer that shifts the dc signal level to provide a 0- to 5-volt analog output. It requires a stable reference voltage, which is supplied by the 2.5-volt low-drift voltage reference, U4. It is also a convenient place to compensate for any residual errors in U2 by adding positive temperature coefficient (PTC) resistors. Resistor 2 decreases the gain as temperature increases, and R3 compensates for zero shift with temperature. The output is clamped by zener diode CR4 to limit it to -0.7 to $+8$ volts in case of a circuit malfunction or failure. If the following electronics can tolerate ± 12 volts without damage, the protective zener and associated resistor could be eliminated.

Temperature Sensor

Late in the program it was decided that knowing the temperature of the instrument package would be of value. This was easily accomplished by adding U5 and U6 and the associated circuitry. The two-terminal temperature transducer, U5, provides a linear 1-microampere-per-kelvin output to amplifier U6. The output of U6 is a 0- to 5-volt output for temperatures from $-60°$ to $+90°$ C. The same circuit could also be used to monitor surface temperatures of a collector or some other device by mounting the temperature sensor remotely. Its stable, linear output that can be scaled to cover any reasonable temperature range makes it ideal for this type of application.

All of the nanoammeter circuitry plus a commercial ± 12 volt power supply was easily assembled on the standard 8.7×9.4 centimeter printed-circuit card. It fits the bottom position of the three-card enclosure under the SVS. Testing was done using a current input from a Keithley picoampere source rather than from a collecting plate as this would be a mission specific item. The collecting plate could be as simple as a piece of printed circuit card having the desired area. The only
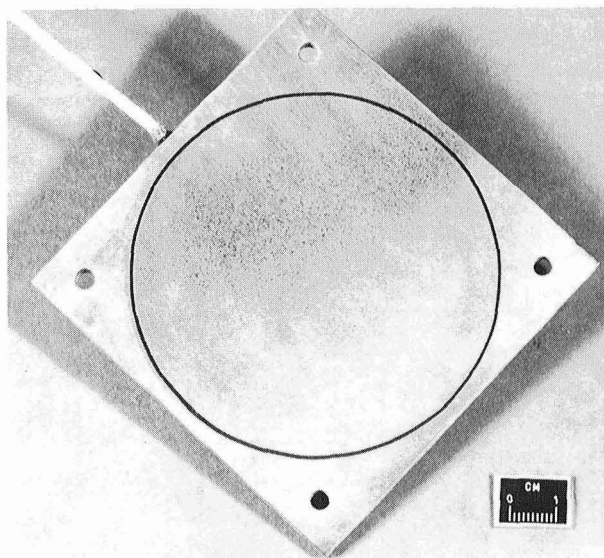

Figure 4. - Experimental collector plate.

requirement is that the sensor and cable be well insulated so that any leakage current is below the lowest current to be measured. An experimental collector plate fabricated in printed circuit card form is shown in figure 4. It has an active area of 50 square centimeters.

Verification and Testing

Test Facility

All three prototype instruments were tested in a glass bell jar system (fig. 5). It is ion pumped with a sorption and sublimation roughing system. Vacuum levels are 10^{-6} to 10^{-7} torr. As shown, the facility is set up to test two SVS's with 2 nanoammeters. They are mounted on a 4.8-millimeter-thick copper baseplate that is temperature controlled. Input current for the nanoammeter is from the 2-picoampere sources in the center of the picture. All data are recorded on the data logger at left, which is operated in a manually controlled scan mode for calibrations and an automatic, once-per-hour scan for long term testing. It records all outputs, input voltage to the surface voltage sensors, primary supply voltage, baseplate temperature, box temperature, temperature sensor output, and time. Temperatures reported were measured near the top of each box and differed by no more than 5° from the baseplate temperature. During testing, the baseplate was heated or cooled to the temperature that brought the box temperature to the desired value. All instruments were tested over a $-40°$ to $+70°$ C range, with power provided by an external laboratory supply.

Figure 5. - Thermal-vacuum test facility.

Test Results

Four nanoammeters were built and tested. One was a breadboard version, and the other three were of nearly flight prototype quality. Each was operated over a current range of 10^{-10} to 5×10^{-5} ampere and at case temperatures from $-40°$ to $+70°$ C. Performances of the four units varied widely. The original breadboard unit showed an almost zero temperature shift over $-20°$ to $+60°$ C and some leakage effects at high temperature for currents below 10^{-9} ampere. The three prototype units were built using components meeting military temperature specifications, where available. Their performances were considerably poorer. The only explanation for this difference in performance is that the log amplifiers came from different lots that had inherently different characteristics.

Analysis of the data for the circuits tested shows that there are two types of error present. One is a gain error, the other a zero shift, and both vary from circuit to circuit. Selective cooling of individual components showed that the ICL8048 produced output shifts at least an order of magnitude greater than any other circuit component. Considering that this is a fairly old integrated circuit, and that it is being used over a wider temperature range than it is rated for, this result is not surprising. At present, it is also the only monolithic logarithmic circuit on the market.

Except for the high-temperature, low-current region, the largest gain change amounted to ± 10 percent of reading or ± 3.5 percent error at the output. A zero shift of 2 percent also occurred. To reduce these errors, temperature compensation of the gain and zero was added. To compensate the zero shift, a Sensitor (a positive temperature coefficient silicon resistor) R3 was added in series with R14. Gain change compensation was made by replacing part of R12 with a Corning nickel film, positive-temperature-coefficient resistor R2. The results were encouraging. The maximum error was reduced to less than one half the previous value. The instrument was still undercompensated so further improvement is possible. Except for the leakage error at high temperatures, the compensated circuit met a ± 5 percent of reading accuracy over its full range. Figure 6 shows the calibration for the nanoammeter incorporating the above modifications.

Measured power consumption of the circuit alone is 102 milliwatts at ± 12 volts dc. A further reduction of power could be achieved by decreasing the supply voltages to as low as $+10$ and -8 volts. When operated with a commercial dc/dc converter, as during the early testing, input power was 450 milliwatts. This was later reduced considerably using a power supply designed for this specifc application. Its design and performance is included in the section after the surface voltage sensor (SVS).

The nanoammeters were thermal-vacuum tested with the SVS for greater than 24 000 unit hours. No failures of any kind occurred, and the calibration remained stable with no time dependent drifts.
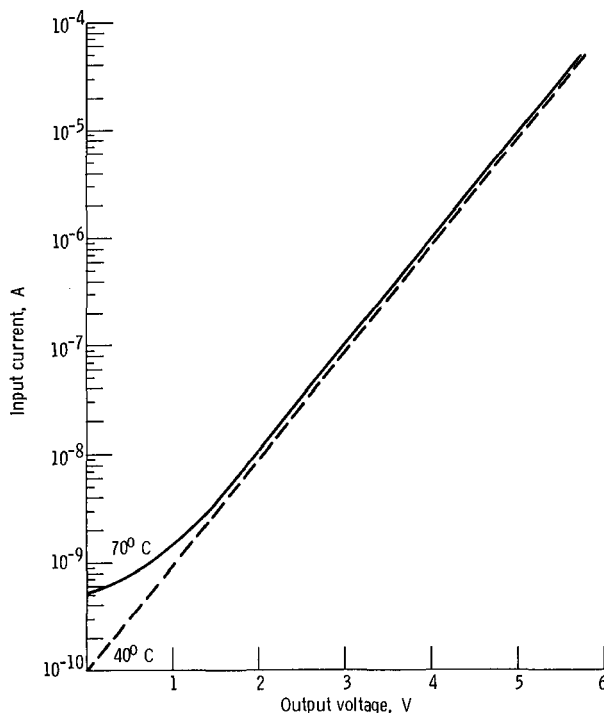
5

Figure 6. - Typical nanoammeter calibration.

Discussion and Conclusions

Calibration shifts with temperature have been shown to depend predominantly on the ICL8048 log amplifier. Two means of eliminating this problem are possible. A tighter selection specification should be applied to the ICL8048, and any remaining shift could then be compensated for with PTC resistors. The latter step could be time consuming, although not nearly as bad as that for previous discrete component logarithmic circuits used to do this function. Overall accuracy of ± 5 percent of reading has been documented. More careful compensation may improve this.

At 70° C and at currents below approximately 5×10^{-9} ampere, the input leakage current of the first stage of some of the ICL8048 amplifiers becomes appreciable. No compensation for this is practical, and the units should be tested for this specification at maximum temperature. At 70° C, the better ICL8048s were usable down to less than 5×10^{-10} ampere.

Other than the above temperature drifts, the nanoammeters have not had any problems or failures. The design is very stable and has been shown to be adequate for its intended use. Flight qualification is the only step remaining to be done.

Surface Voltage Sensor

Requirements

The SVS was required to measure the voltage produced by collected electrons or ions on a well-insulated electrode exposed to the space plasma environment. The measurement technique must not alter the charge of the collecting electrode and must be accurate to within ± 1 percent from $+100$ to $-20\ 000$ volts. Additionally, weight and power consumption were to be minimized. Specifications that were achieved in the prototype units are given in table II.

TABLE II.—SURFACE VOLTAGE SENSOR
SPECIFICATIONS

Range (autoranging), V:
Low .... $+100$ to -2000
High .... 0 to $-20\ 000$
Accuracy, percent...1 or better
Linearity, percent.. $\pm 1/2$ or better
Operating temperature, °C.................................. -40 to $+70$
Temperature drift, percent .... $< \pm 1/2$
Analog and range-bit, V dc ....0 to 5
Range output ....1 digital bit
Electrode diameter, cm 10
Printed circuit card size, cm....................................8.7 by 9.4
Overall size, cm..10.1 by 11.3 by 9.5
Weight (including nanoammeter), kg 0.82
Circuit power ± 12 V dc, mW...195

Design

One of the main factors in the design of the SVS was the requirement of not altering the charge due to ions or electrons collected by the insulated sensing electrode. This dictated that some type of field sensing device be used. Most electrostatic voltmeters that have sufficient accuracy and resolution use a field sensing probe that is closed-loop controlled to the same potential as the surface being measured. In this way the field sensor need only detect a null. To use this approach a "servo-amplifier" with an output of -20 kilovolts would be required, which would be impossible within the weight and power limitations of this instrument.

An alternative approach was selected that retains most of the advantages of a feedback sensing system, yet does not require high voltage. It consists of a combination of electrodes that attenuate the field produced by the sensing surface and allow it to be nulled with a low-voltage feedback signal. A cross section of the SVS sensing head is shown in figure 7. The collector plate is insulated from the rest of the instrument by a ring of Delrin (Acetal homopolymer). No electrical connection is made to this
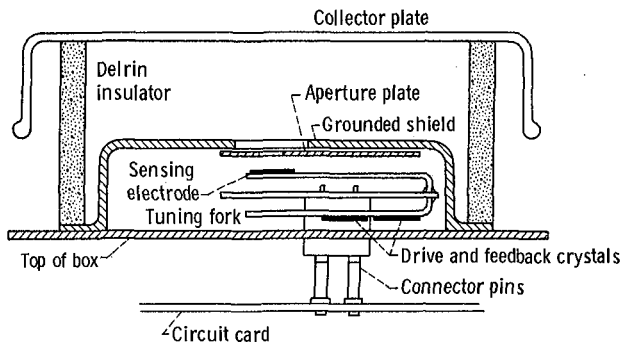
Figure 7. – Surface voltage sensor head detail.

electrode. Creepage paths have been kept long, and the collector plate is shaped to shadow shield the insulator to minimize direct charging of its surface by incident electrons.

Sensing of the field is done using a vibrating electrode driven by a tuning fork. Directly above the sensing electrode is an aperture plate containing a hole through which it can "see" the electrostatic field created by the charge on the top electrode. As it vibrates, it generates a displacement current that is proportional to the net field and at the vibration frequency. The phase of this signal is determined by the polarity of the net field. This field at the sensing electrode is nulled to zero by driving the aperture plate to a voltage inversely proportional to that producing the field. By proper selection of the geometry, particularly the hole size in the aperture plate, this attenuation constant is selected to allow nulling the maximum field with a maximum of 20 volts applied to the aperture plate electrode.

Since two ranges are required for this SVS, the tuning fork carries two separate sensing electrodes made from 0.79-millimeter (0.031-in.) thick printed-circuit card laminate. Each has its corresponding hole in the aperature plate sized so that the low range constant is -100 volts per volt and the high range constant is -1000 volts per volt. The maximum feedback voltage then corresponds to the desired -2- and -20-kilovolts full-scale ranges. The output of the instrument is derived directly from the feedback signal by attenuating it by a factor of 4 to a 0- to 5-volt level.

The only disadvantage of using this field attenuation arrangement is that the calibration is dependent on the exact geometry, which is not true for systems where the full voltage to be sensed is matched. In practice, this requires reasonable mechanical precision and an electrical means of trimming the full-scale voltages. The most sensitive dimension is the diameter of the aperature plate holes. This is because the voltage scaling of the instrument varies at greater than the third power of the hole diameter.

Figure 8 is a block diagram of the SVS. The circuit is basically a servo-amplifier providing an output of 0 to 20 volts for either range, which is used to drive the sensed signal to a null.

In addition to the signal amplifiers, a means of driving the tuning fork is required. To get the maximum amplitude of oscillation with minimum power, the fork should be driven at its self-resonant frequency. This is done by deriving a feedback signal from the motion of the fork and using it to generate the drive. A pair of piezoelectric crystals is used as both drive and feedback elements. The two crystals are mounted on the bottom tine of the fork, the one nearest the base being used as the driver, the one farther out for the feedback. Each is 6.3 by 9.5 by 0.2 millimeter and is made of PZT-5H material. Piezoelectric drive, as opposed to magnetic drive, has the advantage of ease of shielding and no external magnetic fields that might influence other spacecraft instruments.

Mechanical and Tuning Fork Design

The tuning fork that carries the sensing electrodes required considerable design effort. It should have minimum internal damping so it would be easy to drive and not require an excess of power. It must also be strong enough to survive launch vibration without distortion, and preferably nonmagnetic. The design adopted was an electron-beam-welded fork made from 1.0-millimeter (0.04-in.) thick Inconel 718, which was hardened after fabrication. (See fig. 9.) A shield plate, which is also used for mounting, splits the fork symmetrically. This plate provides the isolation necessary between the sensing electrodes, which operate at millivolt levels and very high impedance, and the crystal-drive element, which operates at 36 volts rms. It also makes possible a very effective means of electrical connection to the circuit board. The two signal lines for the sensing disks on the fork go to two coaxial connector pins that are soldered to the shield plate. These lines run along the top surface of the upper tine, across the shield plate, and into the rear of the connector pin. The drive and feedback signals from the crystals are routed along the bottom tine of the fork, across the bottom of the shield plate, and to a connector block carrying three unshielded connector pins. These five pins pass through the top of the enclosure and plug directly into mating pins on the circuit board. Wiring is minimized, and the instrument can be assembled and disassembled easily since no soldered connections need be broken.

The fork assembly is mounted to the enclosure cover on electrical standoffs, which also mount the aperture plate above it. A wire from the aperture

Figure 8. - Surface voltage sensor functional diagram.
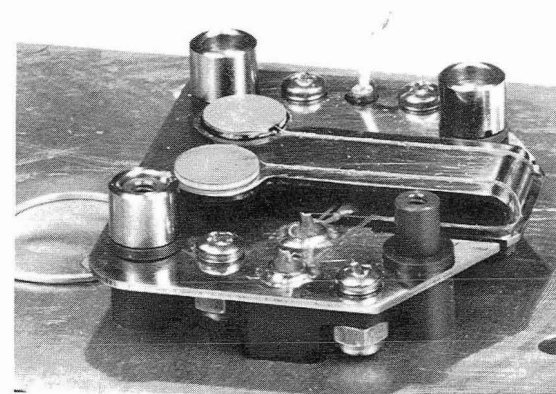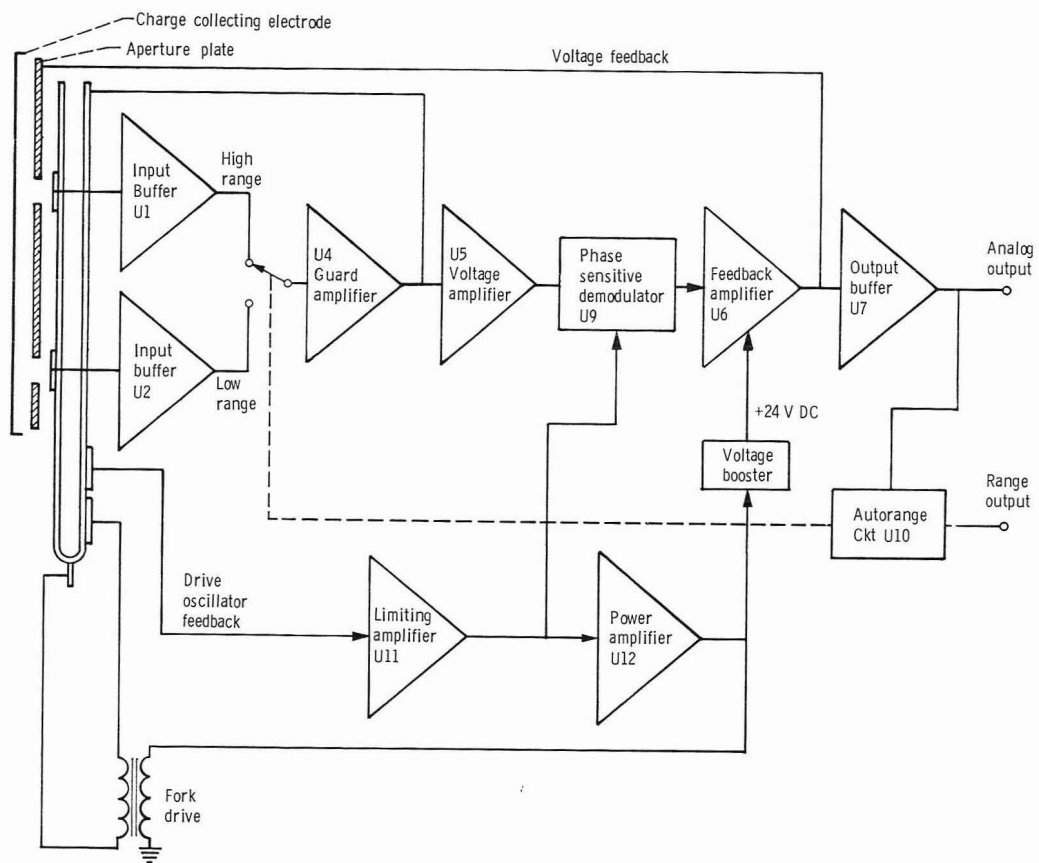
(a) Top view.
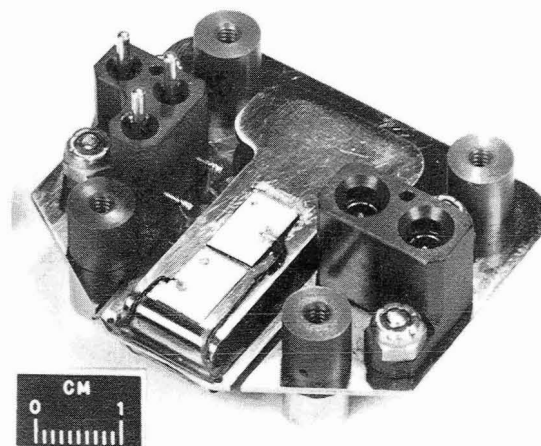
(b) Bottom view.

Figure 9. - Surface voltage sensor fork assembly.

plate connects to one of the pins on the lower side of the fork mounting plate. Figure 1 shows the aperture plate wired to its connector pin and folded back to expose the fork.

Mounted on the cover just in front of the fork assembly is a screened vent port. It is covered with a 165 by 1400 mesh twilled Dutch weave stainless-steel screen. This is the only vent to the tuning-fork enclosure. The screen prevents the entry of contamination, which is important, as any foreign material on the sensing disks or apertures would change its work function and cause a shift in calibration. To provide a surface with a stable work function that will not change with time, the tuning fork, sensing disks, aperture plate, and top electrode are all gold plated.

Circuit Description

The FET input buffer stages are used to match the very high impedance of the sensing electrodes, which are only 9.5 millimeter (3/8 in.) in diameter. The schematic is shown in figure 10. These buffers, U1 and U2 are a custom hybrid circuit that contains a 10 K current limiting resistor, a pair of protective diodes, and a 100-megohm bias resistor plus the FET in a TO18 can. Used alone, it would produce an input load impedance of 100 megohms in parallel with wiring and junction capacitances. To further increase the input impedance, two additional steps have been taken. After the ac input signal is buffered a second time by unity gain amplifier U4, the signal is fed back in phase to the drains of the first stage buffers U1 and U2 by capacitor C1, and is also used to drive the body of the tuning fork on which the sensing electrodes are mounted. Doing this guards the input and decreases the effective capacitance seen at the buffer input.

Selection of the high or low input is made with solid-state switch U3, driven by the autorange circuit. At this point, the millivolt ac signal is buffered by U4 and a small bias voltage added to set the zero output of the instrument. Two zero controls, R18 and R20, set the zero for the two ranges, the proper one being switched in by U3.

The low level signal out of U4 is amplified by a high gain stage U5. Next is a half-wave demodulator U9, which operates as a phase-sensitive detector. Its output is filtered and integrated by U6 to produce the 0- to 20-volt feedback signal to the aperture plate that nulls the sensed field. This signal is inversely proportional to the electrostatic voltage being measured. The feedback signal is attenuated by the network consisting of R14A, R14B, R15, R16, and switch U9. R15 and R16 set the attenuation for the low range. On the high range, solid-state switch U9

closes, allowing the attenuating factor to be trimmed for high-range calibration. In this way it is possible to trim the scale factor for both ranges to produce 0 to 5 volts at the output for the desired full-scale input. The output amplifier U7 is a unity gain buffer which also provides a signal to the autorange circuit. Its output is prevented from going negative by diode D12, which clamps the amplifier output at a low power point.

Tuning Fork Drive

Basic requirements of the fork drive circuit include sufficient gain to start oscillation, a fairly stable output voltage, large power gain, high input impedance, and the generation of a reference square wave to drive the demodulator. The input signal comes from one of the two piezoelectric crystals cemented to the bottom tine of the tuning fork. It produces a feedback signal of 7 volts rms at full oscillation amplitude. This signal is coupled to high-gain amplifier U11 through R37. In normal operation the feedback signal is sufficient to saturate amplifier U11, producing a near-square-wave output from which the demodulator reference signal is derived. This signal is then power amplified by U12, which is a combination active low-pass filter and power stage. It uses a second-order Bessel filter to produce a sine wave from the square-wave input. It also provides most of the 90° phase shift required for the fork to oscillate at its natural resonant frequency. Filtering to a sine wave, while not absolutely necessary to drive the fork, allows the output transformer to operate at a higher voltage level without saturating and decreases potential pickup from drive signal harmonics. Output is a 36-volt-rms sine wave, which drives the crystal nearest the base of the lower fork tine. The output transformer has a 5:1 setup ratio and provides isolation to ground, which is necessary for U4 to drive the fork body with the guard signal.

An additional function is served by the fork drive output. It is used to power a voltage doubler that supplies a boosted 24 volts dc to power feedback amplifier U6. Power required is only a few milliwatts and boosting the supply voltage allows the feedback signal to be 20 volts for full scale. While the SVS could be designed to operate on a lower feedback voltage, and originally was, it would be more susceptible to zero drift.

Demodulator Drive

To drive the demodulator the output of U11 must be corrected to be an exact 50 percent duty cycle and of the proper phase relationship to the error signal.

Notes:
1. Adjust value to trim phasing at synchronous detector.
2. All diodes are 1N916
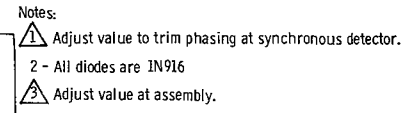3. Adjust value at assembly.

Figure 10. - Surface voltage sensor schematic.

Corrections are made in the network consisting of D5, D13, R24, R25, and C11. Selection of R24 and R25 allows the delay of the rise and fall time of the waveform to be independently controlled. The input of the DG 200AA switch (U9) is C-MOS compatible and presents a high impedance to the compensation circuit. It includes a driver stage that squares up the input before driving the FET switch.

Further phase compensation is required to bring the reference signal into phase with the error signal. In addition to the above network, two other capacitors, C4 and C24, can be trimmed to accomplish this.

Autoranging Circuit

To cover the full −20-kilovolt range and have sufficient resolution to detect a 50-volt charge, it was necessary to make the SVS a dual-range instrument. Switching between ranges is done by an autorange circuit. On the low range, a reference voltage of 4.85 volts is applied to pin 3 of U10 via Q1 and a voltage divider consisting of R29 and R30. When the input signal at pin 2 is lower than this value, its output is at positive saturation, which holds Q1 on. When the output voltage applied to pin 2 exceeds 4.85 volts U10 switches to negative saturation, turning off Q1 and reducing the reference voltage at pin 3 to 0.41 volt now set by R31 and R29. The output, taken after D10 to eliminate the negative voltage swing, range switches the input lines, drives Q2, which provides a T^2 compatible range bit output, and drives the half of U9 which controls the gain for the two ranges.

Verification and Testing

Three complete surface voltage sensors were built for testing. The first showed considerable drift with both time and temperature, and had a tuning-fork frequency about 13 hertz below the other two. X-rays of the area where the two individual tines were electron-beam welded to the center plate showed voids and incomplete weld penetration. An attempt to repair the fork by high-temperature-furnace brazing was only partially successful and that unit never did perform as well as the other two. For this reason the other two units were the ones subjected to the long-term thermal vacuum testing.

Soon after the first model of the SVS was completed, it was recognized that zero drift was its most serious deficiency. The test program was therefore set up to emphasize this measurement. Two prototype units were built and subjected to long-term thermal-vacuum testing in the glass bell jar facility (fig. 5). The two instruments are shown mounted on a temperature-controlled baseplate. They were supplied primary power from an external, laboratory supply via a current metering panel, not shown in the picture. Both sensing surfaces were electrically interconnected, and a lead from them was brought out through a high-voltage feedthrough. A data logger, visible at the upper left, was used to monitor the sensor voltage, output, range output, primary power supply voltage, box temperature, and baseplate temperature for each unit. At the start of the test an additional thermocouple was attached to the case of the internal power supply for the SVS. A chart recorder was also used to monitor the outputs of the SVS's.

Test procedure was to operate the units at a given box temperature over the range of −40° to +70° C with the sensing electrode grounded. Periodically, the electrode was ungrounded and scanned over the full operating voltage, then again grounded. In this way, calibration curves were obtained for all temperatures, as well as a continuous record of the output for zero-input voltage. Data were automatically recorded at 1-hour intervals, except for the calibrations, which took about 20 minutes, and were run between the other data points. Two units were tested in vacuum for over 24 000 unit hours.

Three different power-supply configurations were used during testing. At the start each instrument had its own commercial dc/dc converter type supply. At the low power levels required, these supplies were only 25 to 40 percent efficient. After satisfactory performance with individual supplies was demonstrated, the SVS and nanoammeter were reconnected so that both could operate off one of the supplies used previously. This configuration considerably decreased the total power required because the supply was being used closer to its design rating. Finally, a power supply was designed specifically for the SVS/nanoammeter. It is 80 percent efficient at the design power level of 300 milliwatts and further decreased the required power. Its design and performance are described elsewhere in this paper.

Test Results

Both units were operated successfully without failure except for one of the commercial power supplies and a cold solder joint that opened up during temperature cycling. Comparing calibration curves taken at various temperatures showed that they were perfectly linear and that the slope of the calibration curve, that is, volts out per kilovolt, varied by less than 1 percent as a somewhat predictable function of temperature over the −40° to +70° C range. Most of this error could be compensated for by use of temperature-sensitive resistors in the output buffer circuit in a fashion

similar to that used with the nanoammeter. This was not done, as the uncorrected accuracy is adequate.

Zero shift, both with time and temperature, was the major error source. Testing showed that there was a small zero shift, always in the same direction, that occurred during the first week of operation in vacuum. It reoccurred each time the units were exposed to the atmosphere, indicating outgassing as the probable cause. The maximum shift observed was less than 0.05 percent and decreased as more care was taken in cleaning the sensing head before vacuum testing. The effects of temperature were more pronounced. When operated between the extremes of $-40°$ and $+70°$ C a fairly small zero shift was observed. Considerably larger shifts occurred when the temperature was varied between lesser limits. The step between 28° and $-40°$ C produced the largest output shift—about 50 millivolts or 1 percent of full scale. While these values are acceptable, it should be possible to find the cause and eliminate it.

To this end, a test was run to indicate whether the drift was caused by the mechanical sensing head or by changes in the electronics. The top mechanical assemblies containing the fork, aperture plate, and collection electrode were interchanged between the two SVS units on test. There had been considerable difference in the drift performance of the two units, one having about twice the drift of the other. After the change was made, continued testing showed that the drift performance changed, the higher drift being associated with the same sensing head, regardless of which set of electronics it was connected to. This is a good indication that the drift is at least partly associated with thermal changes in the mechanical assembly.

One change with temperature noted during testing was a shift in fork frequency. Both forks showed a nearly linear decrease of frequency with increasing temperature. The shift was 6.7 hertz over the $-40°$ to 70° C temperature range or 0.06 hertz per C°. This is somewhat greater than the value predicted, based on the change in Young's modulus for the material. The predicted drift was 1 percent, or 4 hertz, using a simplified model of the tuning fork. The effect of thermal expansion was also considered, but is much smaller than the effect of the modulus change.

One fork was mass loaded with wax to lower its resonant frequency and see if a zero shift would result. It did. For a frequency change of 3 hertz, there was a corresponding offset change of 10 millivolts, which is an appreciable fraction of the drift observed during temperature testing.

Electrical causes of zero shift were also investigated. Phase shifts throughout the signal and oscillator circuits were measured, and potential changes with temperature or frequency were evaluated. Coupling capacitors were increased in

several places in the error amplifier circuit so that small changes in operating frequency would not cause a change in phase shift that could be demodulated to produce a dc offset. Only one not easily correctable source of phase shift was found. This is the capacitance of the piezoelectric crystal that provides the feedback signal from the fork. It has a room-temperature value of 7000 picofarads, but its capacitance changes by a factor of 2.5 to 1 over the operating temperature range. A 5000-picofarad capacitor was added across the crystal to stabilize the variation with temperature. Ideally, this added capacitor should have a temperature coefficient opposite that of the crystal, but this was not available and was not tried.

Another possible cause of drift is the large error voltage present at null at the output of U5. It is typically on the order of 1/2 volt, peak to peak. It is in quadrature with the demodulator reference signal and therefore does not produce an error output. The source of this voltage appears to be stray coupling between the fork drive and/or feedback voltages and the high impedance amplifier input. This much pickup is undesirable even though, in theory, it should not affect the performance of the circuit. In practice, any change in coupling with temperature can cause this signal to vary in phase, producing a demodulated output. This signal variation will be fed back causing a shift in operating point to null out this component, thus producing a dc offset or zero shift.

During the course of instrument development, several circuit changes were made that necessitated a redesign of the printed circuit card. As part of this redesign, the layout was changed to minimize stray coupling. Only a small improvement resulted from these changes. Attempts to decrease pickup by adding shielding to the printed circuit card also had little effect. It was possible to decrease the magnitude of the null error signal by one-half by adding a 5-picofarad capacitor between the feedback crystal output and the switch output U3 pin 10. This partially neutralizes some of the pickup but does not appreciably help the zero drift. Taken together, these changes helped lower the zero drift slightly. The indication is that there is still some other drift source present, probably mechanical. The two units extensively tested that included these modifications showed a maximum zero shift, due to all causes, of just over 50 millivolts or 1 percent.

One limitation of the SVS was noted during testing. If a large voltage is applied to the instrument and the connection to the top electrode removed, it will store the charge and continue to read out this voltage. The self-discharge time constant varies with temperature and ranges from about 1/2 to 2 hours, being longest at lower temperatures. A similar effect is evident if the SVS has had a large voltage applied,

which is then discharged. Some charge is retained on the dielectric material which then decays with the same time constant. The effect is small, being no more than 0.8 percent of the applied voltage at room temperature. In use, this charge retention limits the time necessary for the detection of decreases in the incident peak electron voltage. This is not a problem in the intended application. If it did become important, using an insulating material with a somewhat lower resistivity would decrease the self-discharge time constant and therefore decrease the storage or fall time of the instrument.

In space, it is expected that any decrease in peak electron energy will be gradual. This would discharge the sensing electrode by secondary electron emission, preventing it from storing charge for any appreciable time. This effect would not change the charge stored on the dielectric ring.

Measured power drain of the SVS from the ±12-volt power supply was 195 milliwatts.

Discussion and Conclusions

Development of this instrument has been carried to the point of demonstrating its performance under all required conditions other than vibration. Although the packaging was not done to flight specifications, the mechanical constraints necessary for proper operation and stability resulted in a unit that will probably meet flight specifications. If operation in a radiation environment is required, there are several small modifications to the box that will be required. Radiation leaks would occur in the area where the box joins the top and around the connector. Modifications required are minor. At all other spots, shielding is at least equal to the box wall thickness.

Accuracy and drift of the units tested was acceptable but could be improved. Care in the fabrication of the tuning fork assembly, particularly in welding the fork, elimination of the fork frequency shift with temperature, and careful circuit layout, may be all that is required to correct the remaining zero drift problem. Even as presently configured, a ±1 percent accuracy has been demonstrated.

Power Supply Design

As is often the case, the design of a power supply for a new instrument is the last thing to be done. At the time that the design of a suitable power supply for SVS/nanoammeter package was initiated, these instruments had already completed several thousand hours of thermal vacuum testing, and gone through several design changes. The power supply to be reported here was completed late in the program and has been operated with the instruments over the full temperature range and in vacuum for only about 5000 unit hours.

Designing a power supply for an instrument system that has a total power requirement of just under 300 milliwatts at ±12 volts dc can be a challenge, particularly when it is desired to keep the efficiency high. The problem becomes apparent when one examines the power required by the control circuits of typical switching regulators. There are a number of integrated pulse width modulating controls available, but none take less than 7 milliamperes.

At 28 volts input, this amounts to about 2/3 of the output power for the supply, immediately limiting the efficiency to the order of 50 percent for reasonably attainable converter efficiencies. Another way of looking at it is that every milliampere of control current decreases the efficiency by about 9 percent. To obtain the desired efficiency, therefore, demanded an innovative design using the lowest power control components available with a suitable switching regulator. The design was facilitated by the fact that the converter need not operate over a wide range of output powers since the load is constant.

The converter selected for this application was the optimum topology configuration developed by Cuk (refs. 28 to 32). It has a slightly higher parts count than other possible circuits, but has several advantages that led to its choice. These include low output ripple, a single ground referenced switching element, excellent cross regulation, and the ability to operate efficiently over a wide range of input voltages. These features made it practical to use a FET switch having nearly negligible drive power requirements and to eliminate separate output regulators controlling only the +12-volt output and depending on the −12-volt output to follow sufficiently closely. In practice, the plus and minus outputs track within a few millivolts for constant and equal loads. One possible disadvantage of the supply as built is that there is not ground isolation between the input and the output common. It is not an inherent limitation of the converter, but a choice made to simplify the controller. Ground isolation could be added but at a cost in control power and complexity with an attendant decrease in efficiency.

Requirements and Specifications

The specifications met by the power supply are given in table III.

Circuit Design and Operation

A complete circuit diagram of the ±12-volt output

TABLE III.—POWER SUPPLY SPECIFICATIONS

Input voltage (nominal), V dc 28
Input voltage range at 300 mW, V dc ....14 to 40
Reflected input ripple current (peak to peak), mA dc *10*
Switching frequency, kHz...25
Output voltage, V dc .... ±12
Output voltage temperature coefficient, percent/°C......... ≤0.006
Output current, mA:
    Design 12
    Maximum..40
Output regulation (line and load: at +12 V only), mV...............5
Efficiency (for 28 V dc input) above 300 mW output, percent .>80
Ripple and noise, mV, peak to peak maximum.......................10
Operating temperature, °C.................................... −40 to +70
Printed circuit card size, cm ....8.7 by 9.4

power converter is shown in figure 11. It consists of a precision reference source and error amplifier (U1), which pulse-width modulates an astable oscillator (U2) to produce the gate drive for power MOSFET switch (Q_1) in the multiple-output Cuk power stage. The control and reference circuits were designed for minimum power consumption. Use of an XR-L555 CMOS timing circuit as a voltage controlled pulse width modulator and the LM10 low power op-amp and voltage reference resulted in a total control circuit current drain of just under 1 milliampere. This

was one of the major factors contributing to the high overall efficiency of the converter.

Generation of the basic switching waveform is done by the XR-L555 timing circuit. A diode across pins 6 and 7 allows separate control of the charge and discharge of timing capacitor C6, making possible the generation of a less than 50 percent duty cycle output directly. Resistor R7 controls the pulse width and therefore the switch-on time, while R8 controls the pulse spacing. With no control voltage applied, the pulse width is 10 microseconds. It can be controlled by a voltage at pin 5, but can only be decreased because diode D2 blocks an increase in control voltage that would be required to increase the pulse width. Fixing the maximum pulse width does two things. It provides a rough limit on output power and allows the circuit to start inpendent of the control. When power is first applied to the supply, U2 starts oscillating at maximum pulse width. As the output voltage increases to 12 volts, which takes about 7 milliseconds, the control loop starts to decrease the pulse width to maintain regulation. Overshoot at turn-on is no more than 5 percent. Besides limiting in-rush current during turn-on, this type of control prevents the initial error signal from forcing excess pulse widths, which would saturate the input transformer and cause destructive overcurrents.
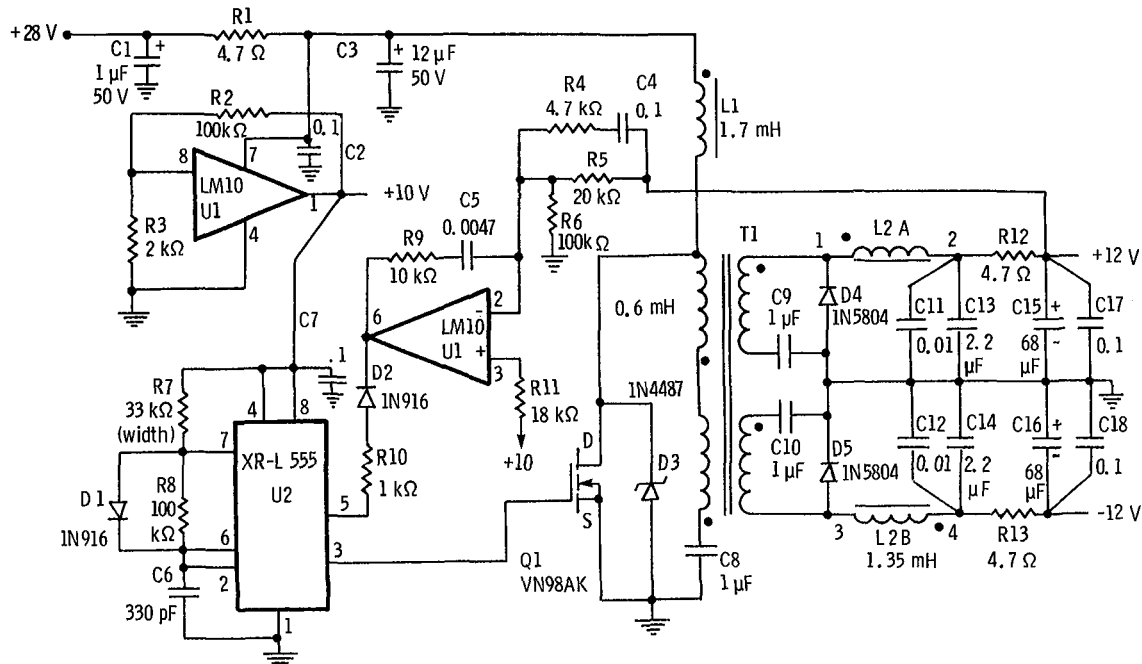
Notes:
    L1 - 90 turns # 30 on 1408P-A100-3B7 core.
    L2 - 150 turns # 30 bifilar on A-050056-2 core.
    T1 - 19 turns # 30 quadrifilar on 1408P-3B7 core.

Figure 11. - ±12-Volt-output-power converter schematic.

When driving the design load, the on and off times are about 4 and 38 microseconds, respectively. Originally, the output of U2 was buffered by several CMOS gates tied in parallel to provide a fast rise and fall time low-impedance drive source to Q1. It was found experimentally that the improved rise and fall times reduced power consumption just enough to be able to detect and it increased the amplitude of the ringing at the FET drain. The driver was eliminated, and at the low power levels involved, the XR-L555 is adequate to drive Q1 directly.

Power for U2 and voltage reference for the error amplifier are provided by one half of the LM10. Its internal 200-millivolt reference signal is amplified to 10 volts for these functions. The other half of the LM10 is used as the error amplifier. It compares a portion of the +12-volt output to the 10-volt reference and drives the modulation input of U2.

One limitation of the control as shown is that the minimum pulse width possible is 1 microsecond. This is not narrow enough to maintain output voltage regulation when the load is removed completely. A minimum load of 80 milliwatts is required.

Since the maximum output power is 1 watt, this results in a usable range of power output of greater than 12 to 1, which is more than adequate for this essentially fixed-load application. If desired, the uncontrolled duty cycle could be set lower, restricting the maximum power output and shifting the operating range downward. The remainder of the circuit is the power converter with its input and output filters.

Several papers describing the operation and design of the Cuk optimum topology converter have been published (refs. 29 to 32), so it will not be discussed in detail here. It functions differently from most switching regulator circuits in that the coupling or energy-transfer element is a capacitor rather than an inductor. It stores energy from the input during the time that the switch (Q_1) is open, and delivers it to the load when Q_1 is closed. In the circuit the transfer capacitor function is fulfilled by a combination of C8, C9, and C10. During the time that Q_1 is off, current flows from the input filter, through inductor L1 and tranformer T1, to charge C8, and by transformer action C9 and C10 through diodes D4 and D5. When switch Q_1 is closed, the energy stored in these capacitors is tranferred to the load. Input current continues to flow through inductor L1, which stores some energy for transfer to the capacitor on the next half cycle. There are capacitors in series with all transformer windings which block the flow of direct current. Thus, there is no possibility of core saturation, operating point creep, or "ratcheting."

One desirable feature of the Cuk converter is that the input and output ripple currents can be made to approach zero by proper coupling of L1, L2A, and L2B. This only applies to the continuous input current mode of operation, which was impractical for this particular application. To achieve continuous input current would require either a large value of inductance for L1 or a high operating frequency. Increasing the inductance of L1 while maintaining very low loss would increase its size and weight appreciably. Increasing operating frequency, which is well within the capability of the FET switch used, would result in higher circuit and magnetic losses. The operating frequency was therefore set at 25 kilohertz, which minimizes losses, and operation was allowed to be discontinuous. The increased ripple was filtered with π input and output filters using resistors for simplicity. The power penalty is almost negligible. Cross regulation was compromised somewhat. This was justified on the basis that the load would be constant, the required regulation was not critical, and the circuit should be as simple as possible. It was possible to combine L2A and L2B on the same core, which provides a factor of two ripple reduction at the output. More important, it eliminates one magnetic component. Large output filter capacitors (68 μF) were necessary to maintain a low output impedance to the large cyclic loading of the SVS fork drive at approximately 400 hertz. The simple control loop used was unable to regulate the effects of this loading.

The complete supply easily fitted on the standard 8.7 by 9.4 centimeter printed circuit card used in these instruments. It is shown in figure 12. Circuit density is not high and, if necessary, it could be built in a smaller area. The full top surface of the board, plus most areas of the bottom, are used as a ground plane to minimize inductance and provide some degree of shielding.

Verification and Testing

Testing of this supply by itself was limited to operating over the full temperature range in air and over the full range of input voltages and output loads. The results of these tests are the basis for the specifications given in table III and the efficiency plots of figures 13 and 14. At the nominal design conditions the efficiency achieved was 80 percent, which is at least double that of any of the commercial supplies tested. After these tests, two converters were installed in the two SVS/nanoammeters, which were then subjected to further thermal vacuum testing over the $-40°$ to $+70°$ C temperature range. Total test time was greater than 5000 unit hours. When operated together off this power supply, the combined SVS/nanoammeter drew a total input power of only 360 milliwatts at 28 volts dc.
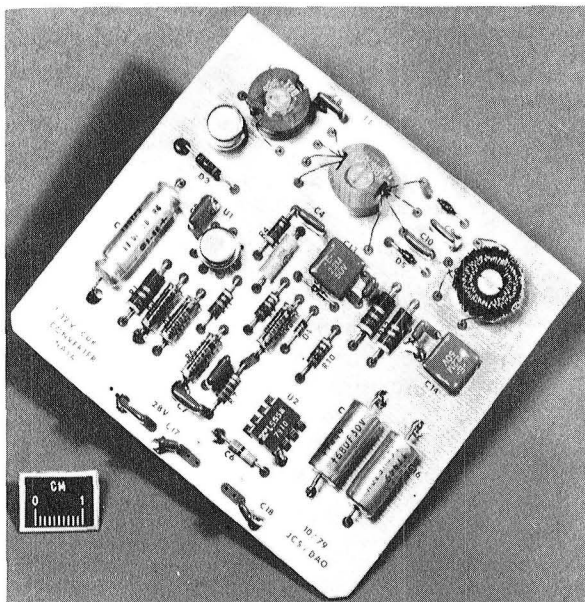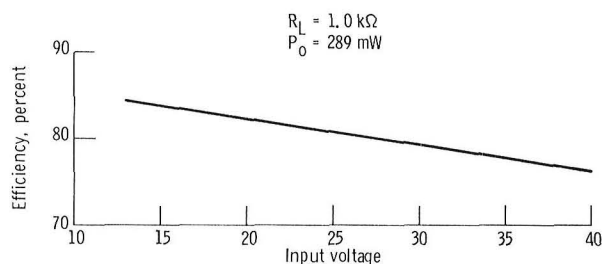
Figure 12. - ±12-Volt power converter.

R_L = 1.0 kΩ
P_o = 289 mW

Figure 13. - Efficiency versus input voltage for ±12-volt converter.
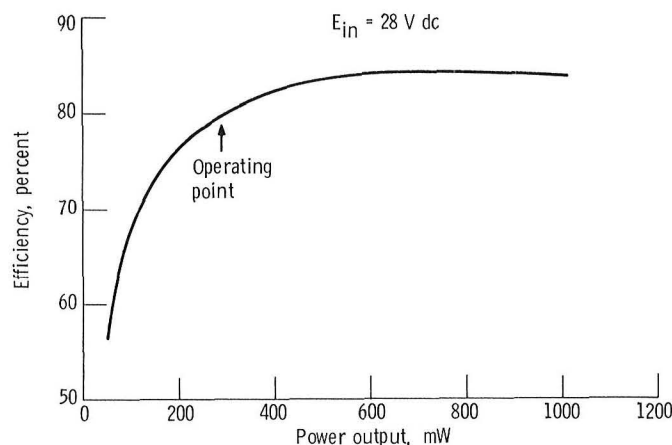

E_{in} = 28 V dc

Operating point

Figure 14. - Efficiency versus power output for ±12-volt converter.

Discussion and Conclusions

A suitable power supply for use at low power levels has been built and tested with very satisfactory results. The efficiency is much higher than any commercially available supplies. Operation with the instruments has been demonstrated over the full −40° to +70° C range in vacuum.

Only one minor problem remains in this design. This is the poor frequency response of the regulator loop at the 400 hertz fork frequency. The addition of a large output filter capacitor circumvented the problem for this application. A more elegant solution would be to improve the regulator loop frequency response, possibly by using a more complex multiloop control. With this modification, the supply could be used for a wide variety of low-power applications, including those having large cyclic loading.

Transient Events Counter

The transient events counter (TEC) was required to sense pulses induced into a spacecraft wiring harness, having amplitudes above a preset threshold. This threshold was to be settable for each channel individually and had to cover the range of amplitudes that might cause false triggering of logic circuits. The full specifications met by the prototype TEC as tested are shown in table IV.

TABLE IV.—TRANSIENT EVENTS COUNTER
SPECIFICATIONS

Electrical sensitivity at input connector:
  Set threshold, V (peak to peak) ....1½ to 8
  Minimum single pulse width[a], nsec...................................20
Dead time[b], minimum, μsec...5
Number of channels (standard configuration) 4
Temperature range, °C.. −40 to +70
Counter capacity, binary bits (255) 8
Count interval.....................Determined by telemetry frame rate
Interface:
  Output, number of bit serial binary for each channel..............8
  Inputs required ....Bit rate clock
                                                          Word length gate
                                                          Frame synch
Circuit power at 13 V dc, mW 273
Primary power requirements (using switching regulator
  supply), mW 380
Printed circuit card size, cm ....8.7 by 9.4
Number of cards ....3 for 4 channels
Overall size, cm...10.1 by 11.3 by 5.4
Weight, kg 0.55

[a]Will count narrower pulses of same energy to <8 ns. Will reliably trigger on 50 MHz damped sine wave.
[b]Longer for large inputs.
[c]All lines T^2 compatible.

Design

TEC III is an improved version of the TEC's flown on the CTS (ref. 27), and the OTS missions. There are several functional differences between TEC III and the previous TEC's. One of the most important is the addition of a precise settable input threshold circuit that will trigger the counter on either positive or negative inputs. It will operate on pulses less than 20 nanoseconds wide.

Another difference is the way in which the counters are read out. Previous TEC's counted up to 63 pulses and reset the counter at the end of each sampling period. This proved to be a problem in actual operation. Most of the time only a few counts or none were recorded during the 4-second counting interval. If noise on the telemetry channel caused a change in count, there was no way to separate the effects. The new circuit does not reset the counter except on power turn on. In this way, if there is an error in the telemetry transmission during one data frame and there are no real counts, the output will return to the previous value on the next data frame.

The other major change over previous units is the input circuit. The TEC III input circuit has been optimized for the fast transients typical of electrostatic discharges and can accept either positive or negative inputs. When a section of blanket insulation has collected enough charge to arc over to ground, it produces a very fast pulse. Typical breakdown voltages are 8 to 15 kilovolts and rise times are less than 5 nanoseconds. Discharge duration is under 0.2 microsecond, so the waveform closely approximates a unit impulse. This impulse couples electrostatically and electromagnetically into the spacecraft structure and wiring. The waveform produced in the wiring harness is a damped sine wave at the resonant frequency of the harness. It is the harness response to a unit impulse. Typical ringing frequencies are 20 to 50 megahertz with amplitudes as high as 50 volts. Damping is usually good and the wave decays in well under 1 microsecond. It is the type of signal the TEC input is optimized for.

Circuit Description

A functional block diagram and detailed electrical schematic of the TEC III are shown in figures 15 and 16, respectively. It consists of two kinds of printed circuit cards. The main card has two complete input and counting channels, and the second card mounts the power supply and telemetry interface circuitry. One or more counter cards could be used with each power supply card to provide the desired number of channels.
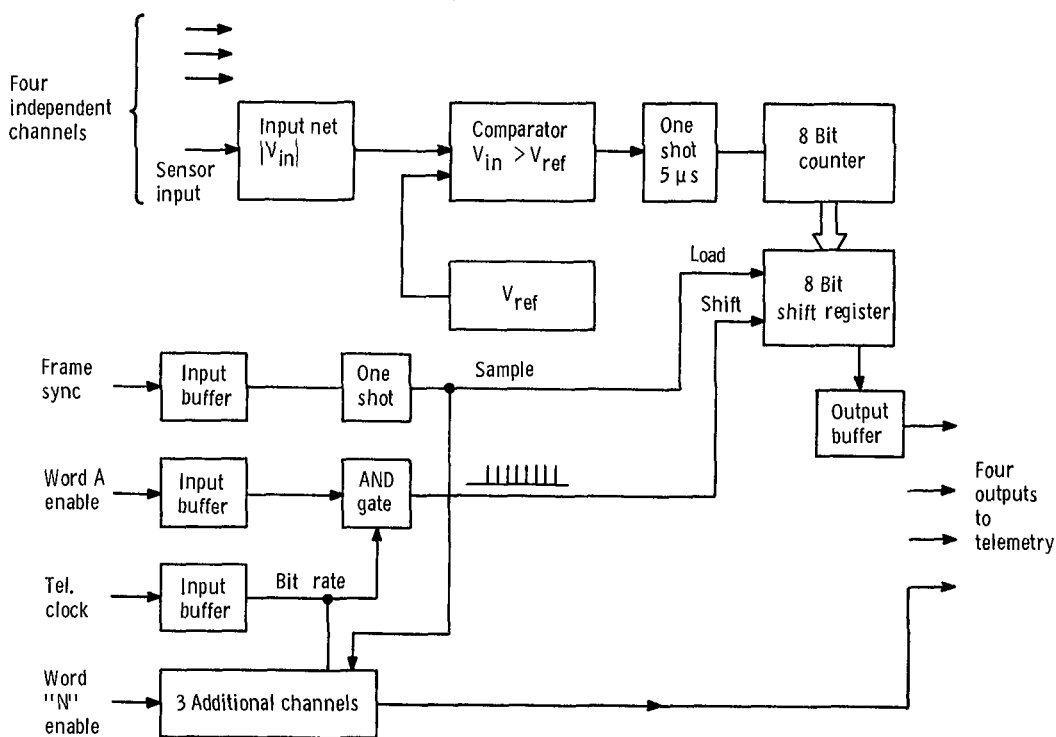

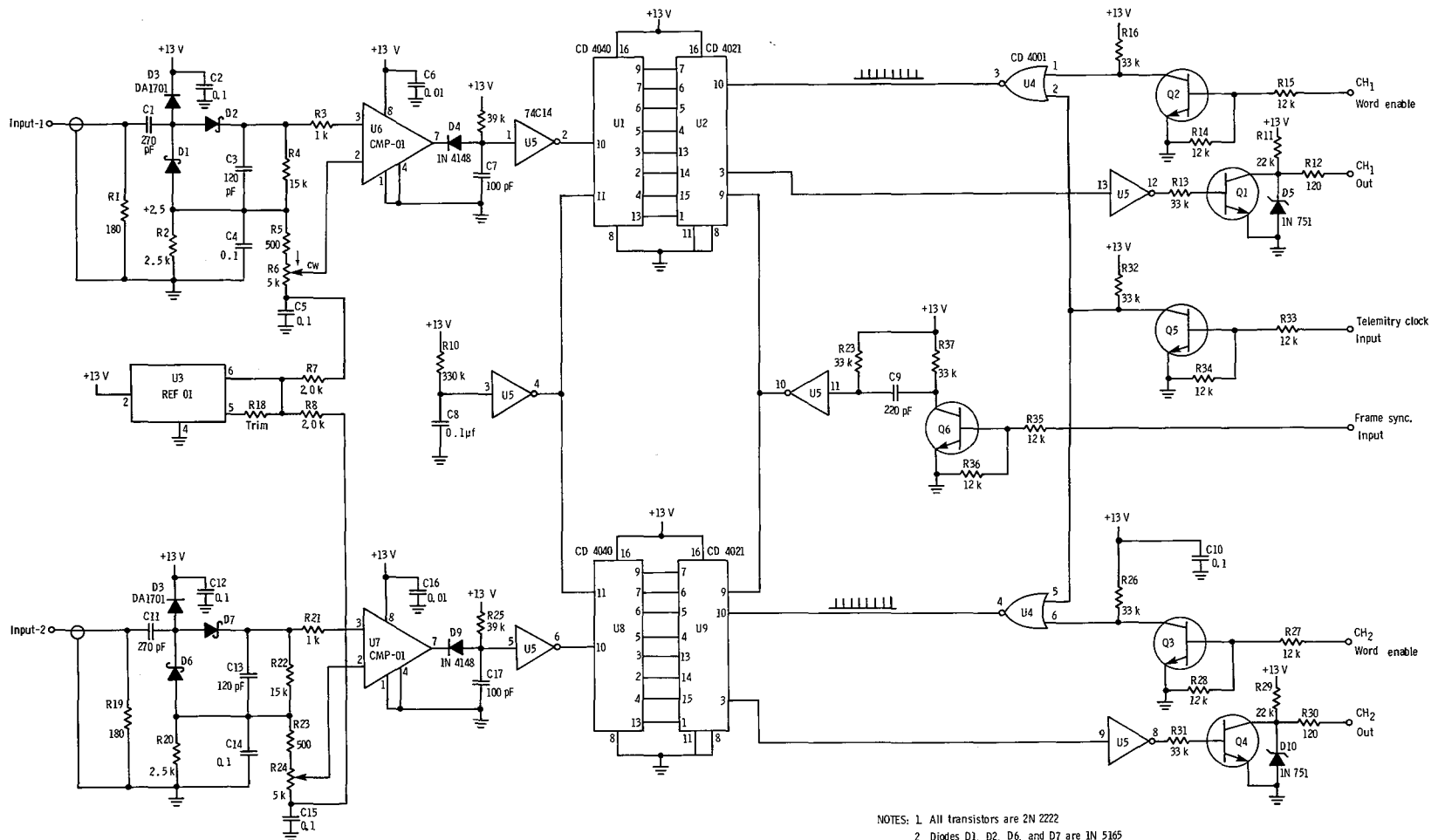Figure 15. - Transient events counter functional diagram.

Figure 16. -Transient events counter schematic.

NOTES: 1. All transistors are 2N 2222
2. Diodes D1, D2, D6, and D7 are 1N 5165

The sensor input is terminated in 180 ohms, a value larger than the characteristic impedance of the cable normally used. The higher resistance is low enough to damp ringing, yet produces a larger signal than a 50-ohm termination would. This input signal is capacitively coupled into a Schottky diode half-wave voltage doubler that effectively produces a positive output proportional to the peak-to-peak amplitude of the input waveform. Thus, the circuit accepts both positive and negative inputs. Comparator U6 changes state when this signal exceeds the threshold set by R6. The input doubler circuit is biased 2.5 volts above ground by current flow through R2. This raises the common mode voltage of U6 above its negative supply terminal, which is connected to ground, enabling it to be operated off the single + 13-volt supply.

When the comparator is triggered, its output drops to ground, discharging C7, which with R9 provides a 5-microsecond or longer stretched pulse to counter U1, via Schmitt trigger U5. Large inputs hold the comparator above its threshold for longer times, lengthening the pulse at its output. Pulse stretching the comparator output prevents multiple counting of waveforms such as fast damped sine wave trains, which are typical for this application. Counter U1 is read out by parallel loading its count into shift register U2. This is done simultaneously to all counters by the telemetry frame sync signal, insuring identical counting intervals for all channels. Each shift register then stores the count until that portion of the telemetry frame when they are read out. At that time, the word-enable line for that counter goes high. Its signal is anded with the telemetry clock in gate U4, producing a series of eight pulses. These shift out the contents of register U2, etc., via Q_1, producing the serial output for that channel. Then Q_1 and Q_4 buffer the C-MOS output to a T^2 compatible output signal. Similarly, transistors Q2, −3, −5, and −6 match the T^2 inputs to the required 13-volt C-MOS internal logic level.

A very stable reference voltage to set the comparator threshold is provided by a precision reference U3. It provides an output of 10.0 volts, which is divided down to the desired set point. If the output of U3 is trimmed down to 9 volts with R18, the power supply voltage can also be reduced to 12 volts if it is desired to use this more common supply voltage.

TEC Switching Regulator Power Supply

All testing of the TEC was done using a commercial power supply. However, to my knowledge, there is no available supply suitable for this application that has a reasonable efficiency at the
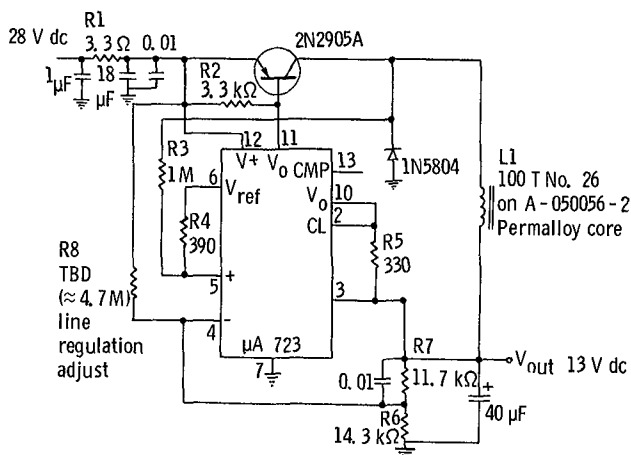

Figure 17. − Transient events counter switching regulator.

low power level required. The circuit of figure 17 is recommended for powering the TEC because it is quite simple, has good efficiency, and is similar to those used on the two earlier TEC's flown on the CTS and OTS missions (ref. 2). A breadboard version of this circuit had an efficiency of 72 percent when outputting 273 milliwatts at 13 volts dc from a 28 volt input. Operating frequency is 83 kilohertz. Using this circuit, the TEC would require 380 milliwatts at 28 volts dc.

Sensors

Considerable flexibility is possible in selecting sensors to couple harness transients into the TEC. When transients in a wiring harness are being monitored, any wire worked into that harness can be used to provide the input. It will capacitively and inductively couple to the harness and provide a signal similar to that induced in the rest of the harness by discharges. This way it is not necessary to make a direct connection to any existing wire or instrument. Previous TEC's used an open ended length of RG178B/U cable with the shield removed on the end 30 to 60 centimeters.

Verification and Testing

Two special pieces of equipment were constructed to facilitate testing. A high-frequency damped sine wave generator and a test box to provide the telemetry timing pulses and clock and to display the output of each channel. The latter is covered in the appendix. The generator used a mercury relay to discharge an L-C circuit and produced the output shown in figure 18. This was used in the threshold and stability tests. A second series of tests was run
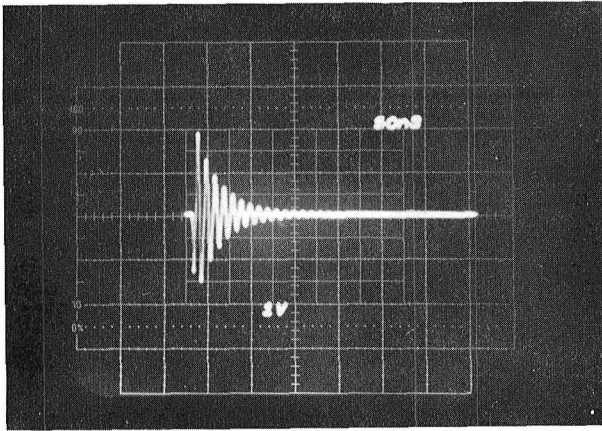
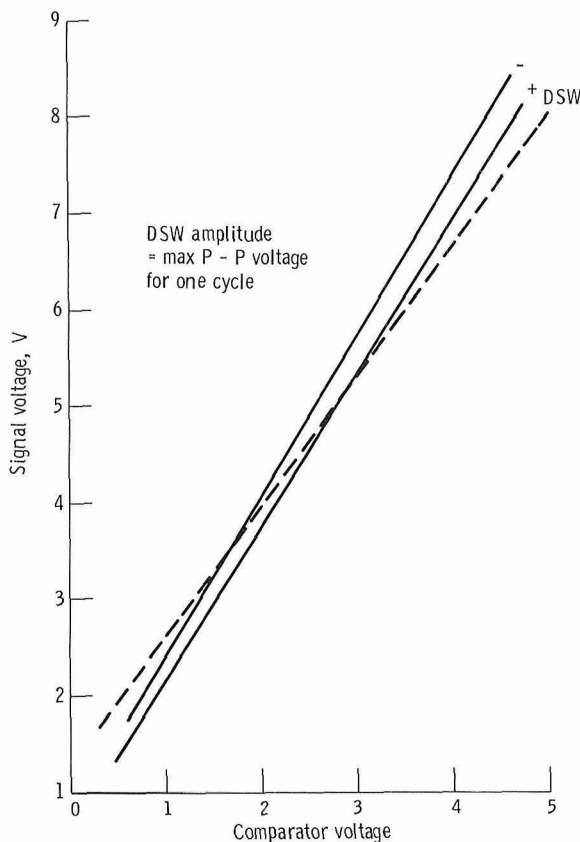Figure 18. - Damped sine wave calibration waveform.

Figure 20. - TEC input trigger sensitivity versus input pulse width.

Figure 19. - TEC input calibration (typical).

required rises somewhat as shown in figure 20. When used to measure discharge induced signals in a wiring harness, the damped sine wave calibration would be the most accurate.

Testing was done in vacuum using a commercial dc-to-dc power converter. The TEC was operated over the full −40° to +70° C temperature range. No operational problems were encountered. There was a small shift in the input threshold. One pair of circuits changed 120 millivolts, the other 90 millivolts from −44° to +69° C. This is less than 1 millivolt per C degree, which can be attributed to the change in forward voltage of the input diodes. It is insignificant for the intended application. Measured power drain of the TEC was 21 milliamperes at 13 volts dc which equals 273 milliwatts.

Discussion and Conclusion

Of the three instruments described in this paper, the TEC III is of the most advanced design, having been preceeded by two flight units. This design incorporates changes found desirable based on previous experience. They are (1) a variable and precisely known input threshold (2) sensitivity to both positive and negative inputs (3) no reset after each data frame (4) decreased power requirements (5) serial digital outputs (6) modular construction facilitating the assembly of units of practically any channel capacity, and (7) an improved box design. This instrument in particular has met all design objectives and is ready for final qualification and use. No modifications or further improvements are suggested except those that might be necessary to adapt its readout to the input requirements of a specific satellite telemetry system.

Common Design Features and Packaging

Since the three instruments were designed to be an add-on package that could be used with any spacecraft, they were designed for minimum weight, power, and volume. They are packaged in two

using positive and negative pulses. Figure 19 shows a typical result using 50-nanosecond pulses and the damped sine wave input. The input threshold stays nearly constant for any pulse width down to about 40 nanoseconds. Below this threshold, the amplitude
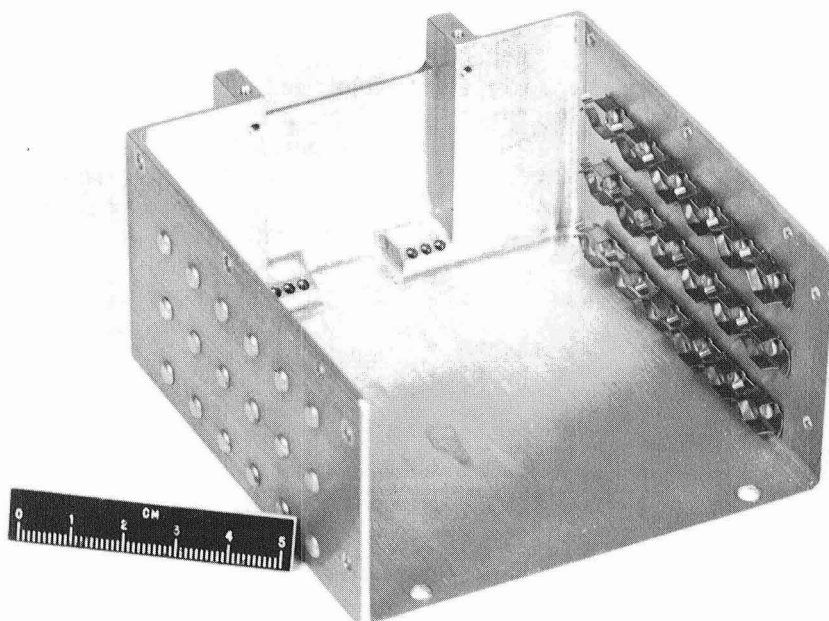
Figure 21. - Electronic printed-circuit card box.

identical electronic boxes (fig. 1) that hold three printed-circuit cards each. Card size is 8.7 by 9.4 centimeters. The cards are retained by beryllium-copper mounting tracks. These have spring fingers that hold the card firmly and provide a good heat-transfer path to the case. Each box is made in three pieces. The main one consists of the bottom, two sides, and the end that mounts the connector (fig. 21). It is machined from one piece of aluminum. The top and remaining end are separate pieces. One of the main advantages of this construction is that the circuit cards can be completely wired together and to the connector and then slid into the box. A vertical wiring duct is formed by the box extension under the connector. This area is also used for the outgassing ports. The SVS must be mounted on the outside surface of the spacecraft and thereby may be subjected to radiation, depending on the orbit. Because of this, conventional screened vents could not be used. Venting is provided by six small holes near the bottom of the wiring duct. They do not go directly through but are drilled from both sides to meet at an angle. In this way radiation shielding at least equal to that afforded by the wall thickness is maintained.

The overall size of the box is 10.1 by 11.3 centimeters on the base, and it is 5.4 centimeters high. An additional 4.1 centimeters in height is required for the sensing head assembly on the SVS for a total height of 9.5 centimeters. The SVS requires only two circuit cards, including one for the power supply, so the logarithmic nanoammeter was packaged with it in the same box. If a common power supply were used, there would be sufficient space for two nanoammeters, should this be desirable. The total weight of the SVS and nanoammeter package is 0.82 kilogram. It is shown both assembled and broken down with the TEC in figure 1. The transient events counter (TEC) requires three cards for a four-channel unit, so it fills its own box. It weighs 0.55 kilogram.

Although these instruments were all designed using flight type construction, they have not been subjected to shock and vibration testing to date. This has been deferred to such time as a specific mission requirement is received. It is believed that the units would pass normal launch shock and vibration conditions as they stand. Thermal testing was done on both instruments. They were successfully operated at temperatures of $-40°$ to $+70°$ C in vacuum.

Lewis Research Center
National Aeronautics and Space Administration
Cleveland, Ohio, January 5, 1981

Appendix—Transient Events Counter Test Set

Unlike the surface voltage sensor and logarithmic nanoammeter, which are self-contained analog output instruments, the TEC must interface with a digital telemetry system. This involves providing several pulse inputs to initiate sampling, determine readout time, shift out the data, and synchronize pulse times. A test set (fig. 22) was built to supply these signals and to provide a visual readout of the four channels. It also provides primary 28-volt dc power to the TEC and has a separate set of buffered outputs on the back that can be used in troubleshooting.

Figure 23 is the timing diagram for the outputs the test set produces, figure 24 is a schematic diagram of the test set. Operation is straightforward. An oscillator output is divided down by counters U11 and U12 to produce the properly sequenced outputs.

These include the frame synchronization pulse, which is 50 microseconds wide and occurs once per second, and a 100-hertz clock of the same width. Gating pulses are supplied in sequence to the four SVS channels. Each is 80 milliseconds wide and is used within the SVS to gate out the eight pulses required to shift the data from the output register. The same gating pulse produces a similar eight pulse train from U2 to shift the data into the 74C164 registers. From these it is outputted in parallel to a readout card that converts it to BCD and drives a three-digit LED display. All internal logic is operated from a 5-volt supply, and all inputs and outputs that interface with the TEC are T^2 compatible. For ease of troubleshooting, all six outputs are separately buffered and made available on the rear panel of the test box.
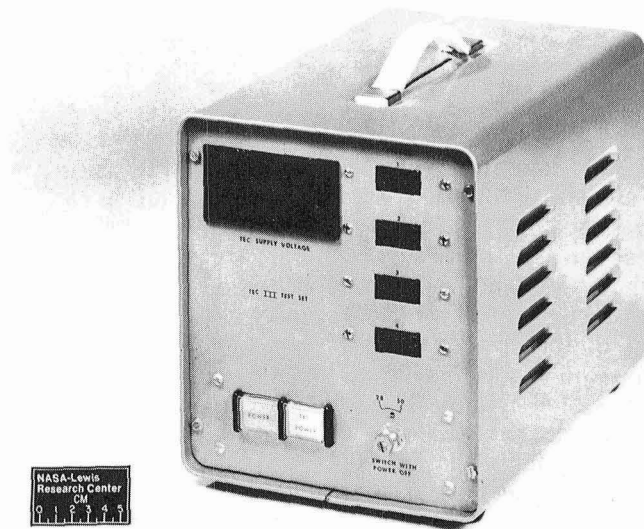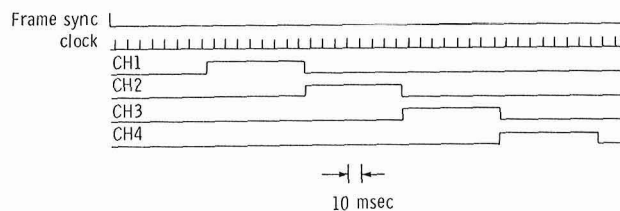

Figure 22. - Transient events counter test set.

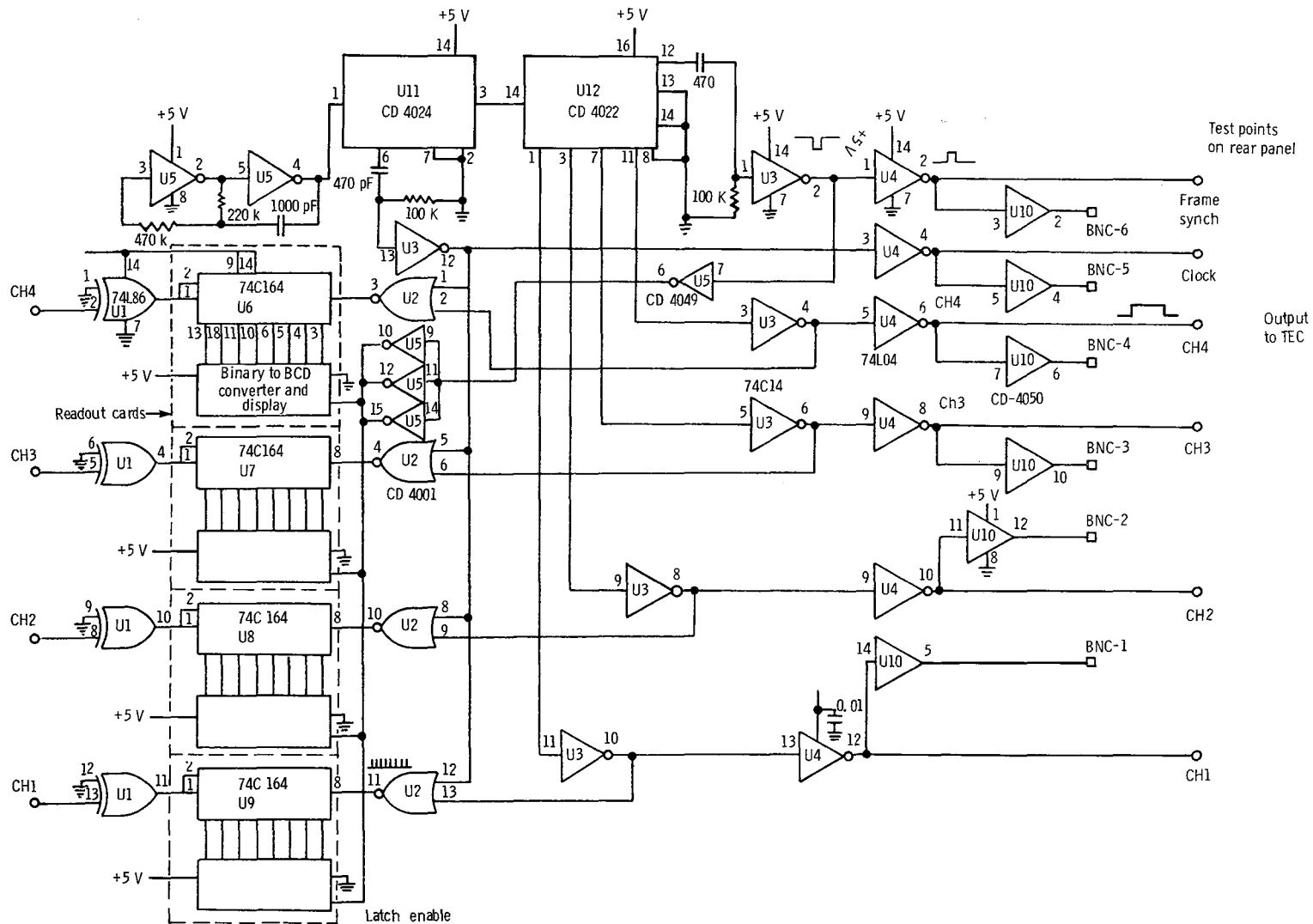Figure 23. - Timing diagram for transient events counter test set.

Figure 24. - Transient events counter test set schematic.

References

1. Rosen, A.; et al.: *RGA Analysis: Findings Regarding Correlation of Satellite Anomalies with Magnetospheric Substorms and Laboratory Test Results.* Report No. 09670-7020-RO-00, TRW Systems Group, 1972.
2. Pike, C. P.; and Bunn, M. H. : A Correlation Study Relating Spacecraft Anomalies to Environmental Data. Spacecraft Charging by Magnetospheric Plasma, Progress in Astronautics and Aeronautics, vol. 47, A. Rosen ed., American Institute of Aeronautics and Astronautics/Massachusetts Institute of Technology Press, 1976, pp. 45-60.
3. DeForest, S. E., Spacecraft Charging at Synchronous Orbits. J. Geophys. Res., vol. 77, Feb. 1972, pp. 651-659.
4. Rosen, A.: *Large Discharges and Arcs on Spacecraft.* Astronaut. Aeronaut., vol. 13, June 1975, pp. 36-44.
5. Fredricks, R. W.; and Scarf, F. L.: Observations of Spacecraft Charging Effects in Energetic Plasma Regions, Photon and Particle Interactions with Surfaces in Space, R. J. L. Grard, ed. D. Reidel Publishing Co., Dordrecht-Holland, 1973, pp. 277-308.
6. Rosen, Alan ed.: Spacecraft Charging by Magnetospheric Plasmas, Progress in Astronautics and Aeronautics, Vol. 47, A. Rosen, ed. American Institute of Aeronautics and Astronautics, Inc., Massachusetts Institute of Technology Press, 1976.
7. DeForest, S.: Spacecraft Charging and Related Effects on Space Structures. AIAA Paper 79-0389, Jan. 1979.
8. Koons, H. C.: Spacecraft Charging—Results from the SCATHA Satellite. Astronaut. Aeronaut., vol. 18, Nov. 1980, pp. 44-47.
9. Wall, J. A.; Burke, E. A.; and Frederickson, A. A. R.: Results of Literature Search on Dielectric Properties and Electron Interaction Phenomena Related to Spacecraft Charging. Proceeding of Spacecraft Charging Technology Conference, C. P. Pike and R. R. Lovell, eds. AFGL TR-77-0051, NASA TM X-73537, 1977, pp. 569-591.
10. Rubin, Allen G.; and Garrett, Henry B.: ATS-5 and ATS-6 Potentials During Eclipse. Spacecraft Charging Technology—1978. AFGL-TR-79-0082, NASA CP-2071, 1979, pp. 38-43.
11. DeForest, S. E.: Electrostatic Potentials Developed by ATS-5. Photon and Particle Interactions with Surfaces in Space, R. J. L. Grard, ed., D. Reidel Publ. Co., 1973, pp. 263-276.
12. Aron, Paul R.; and Stackur, John V.: Area Scaling Investigations of Charging Phenomenia. Spacecraft Charging Technology-1978. AFGL-TR-79-0082, NASA CP-2071, 1979, pp. 485-506.
13. Shaw, R. R.; Nanevicz, J. E.; and Adamo, R. C.: Observations of Electrical Discharges Caused by Differential Satellite-Charging. Spacecraft Charging by Magnetospheric Plasmas. Progress in Astronautics and Aeronautics, Vol. 47, A. Rosen, ed., American Institute of Aeronautics and Astronautics, Inc. Massachusetts Institute of Technology Press, 1976, pp. 61-76.
14. Cauffman, D. P.; and Shaw, R. R.: Transient Currents Generated by Electrical Discharges. Space Sci. Instrum., vol. 1, Feb. 1975, pp. 125-137.
15. Yadlowsky, E. J.; Hazelton, R. C.; and Churchill, R. J.: Puncture Discharges in Surface Dielectrics as Contaminant Sources in Spacecraft Environments. (Colorado State University; NASA Contract NSG-3145.) NASA CR-157105, 1978.
16. Berkopec, F. D.; Stevens, N. J.; and Sturman, J. E.: The LeRC Geomagnetic Substorm Simulation Facility. Proceedings of the Spacecraft Charging Technology Conference, C. P. Pike and R. R. Lovell, eds.

AFGL-TR-77-0051, NASA TM X-73537, 1977, pp. 423-430.
17. Holman, A. B.; and Bunn, M.: Spacecraft Charging Standard Development. Spacecraft Charging Technology-1978. AFGL-TR-79-0082, NASA CP-2071, 1979, pp. 783-796.
18. Stevens, N. J.; Lovell, R. R.; and Gore, V.: Spacecraft Charging Investigation for the CTS Project. NASA TM X-71795, 1975.
19. Stevens, N. John; et al.: Testing of Typical Spacecraft Materials in a Simulated Substorm Environment. Proceedings of the Spacecraft Charging Technology Conference, C. P. Pike and R. R. Lovell, eds. AFGL-TR-77-0051, NASA TM-73537, 1977, pp. 431-457.
20. Purvis, C. K.; Stevens, N. J.; and Oglebay, J. C.: Charging Characteristics of Materials: Comparison of Experimental Results with Simple Analytical Models. Proceedings of the Spacecraft Charging Technology Conference, C. P. Pike and R. R. Lovell, eds. AFGL-TR-77-0051, NASA TM-73537, 1977, pp. 459-486. Also NASA TM X-73606, 1977.
21. Reddy, J.; and Serene, B. E.: Effects of Electron Irradiation on Large Insulating Surfaces Used for European Communications Satellites. Spacecraft Charging Technology Conference-1978. AFGL-TR-79-0082, NASA CP-2071, 1979, pp. 570-586.
22. Adamo, R. C.; and Nanevicz, J. E.: Spacecraft-Charging Studies of Voltage Breakdown Processes on Spacecraft Thermal Control Mirrors. Spacecraft Charging by Magnetospheric Plasmas, Progress in Astronautics and Aeronautics, Vol. 47, A. Rosen, ed. American Institute of Aeronautics and Astronautics, Inc./Massachusetts Institute of Technology Press, 1976, pp. 225-235.
23. Durrett, J. C.; and Stevens, J. R.: Description of the Space Test Program P78-2 Spacecraft and Payloads. Spacecraft Charging Technology Conference-1978. AFGL-TR-79-0082, NASA CP-2071, 1979, pp. 4-10.
24. Lovell, R. R.; et al.: Spacecraft Charging Investigation; A Joint Research and Technology Program. Spacecraft Charging By Magnetospheric Plasmas, Progress in Astronautics and Aeronautics, vol. 47, A. Rosen, ed. American Institute of Aeronautics and Astronautics, Inc./Massachusetts Institute of Technology Press, 1976, pp. 3-14.
25. McPherson, D. A.; Cauffman, D. P.; and Schober, W.: Spacecraft Charging at High Altitudes—The SCATHA Satellite Program. AIAA Paper 75-92, Jan. 1975.
26. Berkopec, F. D.; Stevens, N. J.; and Sturman, J. C.: The Lewis Research Center Geomagnetic Substorm Simulation Facility. NASA TM X-73602, 1976.
27. Stevens, N. J.; Klinect, V. W.; and Gore, J. V.: Summary of the CTS Transient Event Counter Data After One Year of Operation. IEEE Trans. Nucl. Sci. vol. NS-24, Dec. 1977, pp. 2270-2275. NASA TM-73710, 1977.
28. Cuk, Slobodan: *Modelling, Analysis, and Design of Switching Converters.* Ph.D thesis, California Institute of Technology, Nov. 1976.
29. Cuk, Slobodan; and Middlebrook, R. D.: A New Optimum Topology Switching DC-to-DC Converter. IEEE Power Electronics Specialists Conference-1977 Record, Institute of Electrical and Electronics Engineers, Inc., 1977, pp. 160-179
30. Cuk, Slobodan; and Middlebrook, R. D.: Coupled-Inductor and Other Extensions of a New Optimum Topology Switching DC-to-DC Converter. IEEE Industry Applications Society Annual Meeting-1977 Conference Record, Institute of Electrical and Electronics Engineers, Inc., 1977, pp. 1110-1126.
31. Cuk, Slobodan: *Switching DC-to-DC Converter with Zero*

Input or Output Current Ripple. IEEE Industry Applications Society Annual Meeting–1978 Conference Record, Institute of Electrical and Electronics Engineers, Inc., 1978, pp. 1131–1146.

32. Middlebrook, R. D.; and Cuk, Slobodan: Isolation and Multiple Output Extensions of a New Optimum Topology Switching Dc-to-Dc Converter. PESC'78; Power Electronics Specialists Conference, L. Ogborn, ed. Institute of Electrical and Electronics Engineers, Inc., 1978, pp. 256–264.

1. Report No. NASA TP-1800	2. Government Accession No.	3. Recipient's Catalog No.
4. Title and Subtitle DEVELOPMENT AND DESIGN OF THREE MONITORING INSTRUMENTS FOR SPACECRAFT CHARGING		5. Report Date September 1981
		6. Performing Organization Code 505-55-7A
7. Author(s) John C. Sturman		8. Performing Organization Report No. E-603
		10. Work Unit No.
9. Performing Organization Name and Address National Aeronautics and Space Administration Lewis Research Center Cleveland, Ohio 44135		11. Contract or Grant No.
		13. Type of Report and Period Covered Technical Paper
12. Sponsoring Agency Name and Address National Aeronautics and Space Administration Washington, D.C. 20546		14. Sponsoring Agency Code

15. Supplementary Notes

16. Abstract

A set of instruments has been developed that can provide early detection of potentially dangerous geomagnetic substorm conditions and monitor the spacecraft response. The set consists of a sensor that measures the characteristic energy of collected electrons or ions from +100 to -20 000 V, a logarithmic current density sensor that measures local electron flux by measuring currents from 10^{-9} to 10^{-5} A, and a transient events counter that counts the spurious pulses from electrostatic discharges that couple into the spacecraft wiring harness. The counted pulses are those that are large enough to cause circuit malfunction. Design details and performance characteristics of the three instruments are given. Size, weight, and power requirements have been minimized. Total weight and power for all three instruments is 1.36 kg and 0.75 watt. The instruments are also suitable for laboratory use.

17. Key Words (Suggested by Author(s)) Spacecraft charging; Surface voltage sensor; Nanoammeter; Transient events counter; Electrical discharges; Electrostatic voltmeter	18. Distribution Statement Unclassified - unlimited STAR Category 19	
19. Security Classif. (of this report) Unclassified	20. Security Classif. (of this page) Unclassified	21. No. of Pages 28	22. Price* A02

*For sale by the National Technical Information Service, Springfield, Virginia 22161

National Aeronautics and
Space Administration

Washington, D.C.
20546

NASA

POSTMASTER: If Undeliverable (Section 158
Postal Manual) Do Not Return